

## Systematic errors in ground heat flux estimation and their correction

P. Gentine,<sup>1</sup> D. Entekhabi,<sup>2</sup> and B. Heusinkveld<sup>3</sup>

Received 2 November 2010; revised 8 August 2012; accepted 9 August 2012; published 22 September 2012.

[1] Incoming radiation forcing at the land surface is partitioned among the components of the surface energy balance in varying proportions depending on the time scale of the forcing. Based on a land-atmosphere analytic continuum model, a numerical land surface model, and field observations we show that high-frequency fluctuations in incoming radiation (with period less than 6 h, for example, due to intermittent clouds) are preferentially partitioned toward ground heat flux. These higher frequencies are concentrated in the 0–1 cm surface soil layer. Subsequently, measurements even at a few centimeters deep in the soil profile miss part of the surface soil heat flux signal. The attenuation of the high-frequency soil heat flux spectrum throughout the soil profile leads to systematic errors in both measurements and modeling, which require a very fine sampling near the soil surface (0–1 cm). Calorimetric measurement techniques introduce a systematic error in the form of an artificial band-pass filter if the temperature probes are not placed at appropriate depths. In addition, the temporal calculation of the change in the heat storage term of the calorimetric method can further distort the reconstruction of the surface soil heat flux signal. A correction methodology is introduced which provides practical application as well as insights into the estimation of surface soil heat flux and the closure of surface energy balance based on field measurements.

**Citation:** Gentine, P., D. Entekhabi, and B. Heusinkveld (2012), Systematic errors in ground heat flux estimation and their correction, *Water Resour. Res.*, 48, W09541, doi:10.1029/2010WR010203.

### 1. Introduction

[2] The components of the Earth's surface energy balance are key drivers of the dynamics of the Earth's major cycles (water, energy and biogeochemical cycles). Furthermore the energy balance equation is used to determine the internal energy state or the temperature of the ground and canopy bodies. The land surface energy balance equation is

$$R_n - G(z) - \frac{dS}{dt} = H + \lambda E, \quad (1)$$

here  $R_n$  is the instantaneous net radiation,  $G(z)$  is the soil heat flux at depth  $z$ ,  $S$  represents the storage term in the soil and air within the measurement depth/height,  $H$  is the sensible heat flux,  $\lambda E$  is the latent heat flux and  $t$  is time. If vegetation heat storage is negligible, the surface soil heat flux (heat conduction into the soil right at the surface  $z = 0$ ) may be written as the sum of the soil heat flux at depth and the soil storage term:  $G_0 = G(z) + dS/dt$ .

<sup>1</sup>Department of Earth and Environmental Engineering, Columbia University, New York, USA.

<sup>2</sup>Ralph M. Parsons Laboratory, Massachusetts Institute of Technology, Cambridge, Massachusetts, USA.

<sup>3</sup>Meteorology and Air Quality Group, Wageningen University, Wageningen, Netherlands.

Corresponding author: P. Gentine, Department of Earth and Environmental Engineering, Columbia University, 500 W. 120th St., New York, NY 10027, USA. (pg2328@columbia.edu)

[3] In this study our focus is on the estimation of the surface soil heat flux in both the modeling and observational contexts. We demonstrate that there are some practical issues that can cause errors in the measurements of the flux. Furthermore the numerical modeling of the flux in discretized systems can also lead to problems related to capturing essential high-frequency dynamics that are important to the overall surface energy balance.

[4] The representation of the soil heat flux here refers to sensible heat conduction only and it does not include latent heat conduction or heat convection by liquid or vapor moisture flow. However the numerical model used in this study for testing includes these terms.

[5] The motivation for this study is the recognition that in situ measurements of the surface energy balance components often result in closure errors amounting to about 10% to 30% of net radiation [Wilson *et al.*, 2002]. There are multiple factors that contribute to the improper surface energy balance closure. There are large differences in the sensing areas (footprint) or volumes represented by each sensor. Furthermore each instrument has some practical constraints for their placement that lead to biased sampling with shifted phase or modulated amplitude errors. Additionally, discrete spatial and temporal sampling introduces a band-pass-filtered version of the energy budget. This filtered version can be written as

$$F_{R_n}(R_n) - F_{G_0}(G_0) = F_H(H) + F_{\lambda E}(\lambda E) + IB, \quad (2)$$

in which  $F_X$  represents a band-pass filter applied to the flux  $X$  and  $IB$  represents the imbalance resulting from the filtering.

For instance, the limited high-frequency response of the sensors introduces a low-pass filter. The definition of a flux averaging period similarly introduces a high-pass filter [see *Stewart and Thom, 1973; Spittelhouse and Black, 1981; Foken and Oncley, 1995; Massman and Lee, 2002; Heusinkveld et al., 2004*]. Since the filters are different for each flux and may be nonlinear, their combination usually result in an imbalance that is difficult to detect and mitigate.

[6] In situ measurements of net radiation are relatively precise so that the measured net radiation should be expected to be a good approximation of the actual signal:  $F_{R_n}(R_n) \approx R_n$  [*Jackson et al., 1985*].

[7] Measurements of turbulent heat fluxes at the land surface have undergone tremendous progresses in recent decades with the development of new technologies such as fast-response eddy correlation sensors [e.g., *Baldocchi et al., 1988; Eugster et al., 1997; Ibrom et al., 2007*] or scintillometry [*Chehbouni et al., 2000; Beyrich et al., 2002; Meijninger et al., 2002; Ezzahar and Chehbouni, 2009*]. Several correction methodologies have been developed to correct the raw eddy correlation or scintillometry data [*Webb et al., 1980; Green and Hayashi, 1998; Massman, 2000; Meijninger and De Bruin, 2000; Paw et al., 2000; Twine et al., 2000; Massman and Lee, 2002*] so that the mismatches between the measured turbulent heat fluxes  $F_H(H)$ ,  $F_{\lambda E}(\lambda E)$  and the actual fluxes  $H$ ,  $\lambda E$  are minimized.

[8] The soil heat flux has not received as much attention as the turbulent heat fluxes for several reasons. Soil heat flux measurements are inherently difficult because the sensors must be buried in the ground. The positioning of these instruments is constrained by practical considerations [*Horton and Wierenga, 1983a; Heusinkveld et al., 2004*]. The estimation of a surface soil heat flux that is applicable in (1) is often not achieved with instruments that are buried deeper in the ground [*Heitman et al., 2008a, 2008b; Sakai et al., 2011*]. Soil heat flux sensors can introduce important heat flow distortion induced by the difference in conductivity between the plates and the surrounding soil, poor contact between the sensors and the soil, alteration of the heat flux by liquid and vapor water movement, etc. All contribute to errors in the estimated surface heat flux [see *Philip, 1961; Fuchs and Hadas, 1973; Mayocchi and Bristow, 1995; Sauer et al., 2003; Ochsner et al., 2006; Sauer et al., 2008; Heitman et al., 2008a, 2008b, 2010*].

[9] In addition, soil heat flux has often been perceived as a second-order term in the surface energy budget, especially in the presence of full vegetation cover. However during the day, soil heat flux transitions between near-equal positive and negative peaks (barring passage of synoptic weather). As a consequence instantaneous soil heat flux can be large and a significant component of the surface energy balance even in the presence of vegetation cover [*Gao, 2005; Kun and Wang, 2008*].

[10] The diurnal response of the sensible surface soil heat flux  $G_0$  has been recently revisited from experimental [*Heusinkveld et al., 2004*] and analytical [*Gentine et al., 2010, 2011*] points of view. These studies demonstrate that the signal characterizing the response of  $G_0$  is rich in high frequencies (temporal). The signal contains short-period dips and spikes that are significant to the surface energy balance closure.

[11] Both model and observational evidence point toward the fact that in frequency domain the surface soil heat

flux  $G_0$  is essentially a high-pass filter of and phase shift operator on incoming radiation. Incoming radiation is defined as

$$I_{\downarrow} = (1 - \alpha_s)S_{\downarrow} + L_{\downarrow}, \quad (3)$$

where  $S_{\downarrow}$  is the incident shortwave radiation,  $L_{\downarrow}$  is the longwave radiation from the atmosphere and  $\alpha_s$  is the surface shortwave albedo.

[12] The consequences of this behavior have been partially reported by *Fuchs and Hadas [1972]*, *Idso et al. [1975]*, and *Santanello and Friedl [2003]*. The phase difference, as well as the variations in gain amplitude as a function of frequency, fundamentally preclude the use of simple parameterizations for soil heat flux such as those that take the ground heat flux to be a fraction of the net radiation [*Murray and Verhoef, 2007a, 2007b; Santanello and Friedl, 2003*] or the force restore approach to soil heat flux modeling [*Gentine et al., 2011*]. The objective of this work is to demonstrate the consequences of the predominance of high frequencies in the sensible surface soil heat flux signal. We thus argue that some of the observed imbalance  $IB$  of the surface energy budget can be attributed to the filtering of the actual surface soil heat flux signal  $F_{G_0}(G_0)$  by attenuation of the high-frequency component of  $G_0$ .

[13] The first part of this study introduces an analytical continuum land-vegetation-atmosphere model, which is used to gain physical insights into the heat propagation near the soil surface at all temporal frequencies including the high frequencies that are missed in discretized numerical modeling. A long-term field data set and a calibrated high vertical resolution soil-vegetation-atmosphere transfer (SVAT) numerical model output are used to further evaluate other aspects of the study focus. Using the models and data set we show that there is a loss of information about the surface heat flux in current measurement and estimation methods. This has important implications for the goal of achieving surface energy balance closure. A correction methodology is introduced for typical field observations that provides practical application. Finally, the effect of the temporal sampling for the measurements or modeling of soil heat flux is shown to be a significant factor in the surface energy balance closure especially under intermittent cloudy conditions.

## 2. Approach

### 2.1. Soil–Vegetation–Atmospheric Boundary Layer Analytical Model

[14] A simplified analytical model of the soil–vegetation–atmospheric boundary layer (ABL) continuum [*Gentine et al., 2010, 2011*] provides the framework to explore the gain amplitude and phase spectra of the temperature and heat flux profiles in the soil and in the surface air layer. The analytical model captures the continuous vertical profile and the continuous time record of the states and fluxes. This is in contrast with numerical models that filter the states and fluxes in proportion to their discretization. In the analytical model the soil temperature and heat flux profiles and the surface air layer temperature and heat flux profiles both

respond dynamically and with two-way coupling to incoming radiation (see Figure 1).

[15] The analytical model is not meant to be a complete representation for operational use; it is used to gain insight into the relevant processes and to highlight the emergent behavior of the coupled land-ABL system, especially the phase and amplitude propagation of states and fluxes in the media. The amplitude and phase spectra can be evaluated at all frequencies and the functional dependence on model parameters can be isolated. The main limitations of the model are that (1) it only resolves the sensible heat flux in the soil profile, (2) it does not resolve the subdiurnal variations in soil moisture (a fixed value of soil moisture has to be prescribed each day, modifying the water availability for evapotranspiration and the soil thermal properties), and (3) the model assumes a uniform soil thermal diffusivity. *Gentine et al.* [2010, 2011] provides more detail on the model design and report on its testing against field measurements.

## 2.2. SUDMED Data Set

[16] For observation-based tests we use the SUDMED (Sud-Mediterranean) 2002 field campaign data set [*Duchemin et al.*, 2006; *Gentine et al.*, 2007; *Chehbouni et al.*, 2008]. The field campaign, which spans 101 days, was conducted in the semiarid region of Marrakech, Morocco. The study site cover is sparse cropped wheat that has marked seasonal phenology. We use observations from the R3 site, which is located within an irrigated area in the Haouz plain surrounding Marrakech. The data set covers a wide range of environmental and surface conditions with air temperature ranging from 0°C in the winter to 50°C in the summer and LAI ranging from 0 (sowing) to more than 5 before harvest. Almost all of the annual precipitation occurs in winter and spring [see *Duchemin et al.*, 2006; *Gentine et al.*, 2007; *Chehbouni et al.*, 2008]. The cumulative precipitation is generally on the order of 250 mm per year.

[17] The surface energy balance components were continuously monitored starting 4 February (day of year (DOY) 35) until 21 May (DOY 141), lasting the entire wheat cultivation season. Significant vegetation cover emerged around 7 February (DOY 38), with a growth peak on 20 April (DOY 110), followed by the senescence period until the end of May. Near-continuous measurements were made during the entire wheat season.

[18] Sensible heat flux was measured with a 3-D sonic anemometer (CSAT3, Campbell Scientific, Logan, Utah) at 3 m height. A KH<sub>2</sub>O krypton hygrometer measured the latent heat flux at the same height. The soil heat flux was monitored with three HFP01 Hukseflux heat flux plates buried at 1 cm below the surface, two plates buried at 10 cm and one plate buried at 30 cm. Soil heat flux was recorded at a 30 min temporal resolution. The net radiation was monitored with a CNR1 located at 2 m above the ground. Volumetric soil moisture was monitored with several calibrated Time Domain Reflectometry Campbell CS600 sensors (TDRs) located at 5, 10, 20, 30, 40, 50 cm below the surface (one single measurement per depth). Soil temperatures were measured by Campbell 108B thermistors at 1, 5, 10, 20, 30 and 50 cm at a 30 min resolution.

[19] The data were averaged and stored at 30 min intervals, except for the turbulent heat fluxes which were also stored at the initial sampling frequency of 10 Hz and averaged over 10 min intervals. Suspect measurements were removed from the data set, i.e., sensible heat flux larger than 400 W m<sup>-2</sup> or smaller than -150 W m<sup>-2</sup>, latent heat flux larger than 600 W m<sup>-2</sup> and smaller than -50 W m<sup>-2</sup>. Temperatures outside of -5°C and 50°C were also removed. The removed and missing data were replaced with spline-interpolated values. Less than 2% of data were missing. The average energy balance closure between the measured turbulent heat fluxes  $H + \lambda E$  and the measured available energy using the soil heat flux at 1 cm,  $R_n - G_{1\text{cm}}$ , was 79% and the

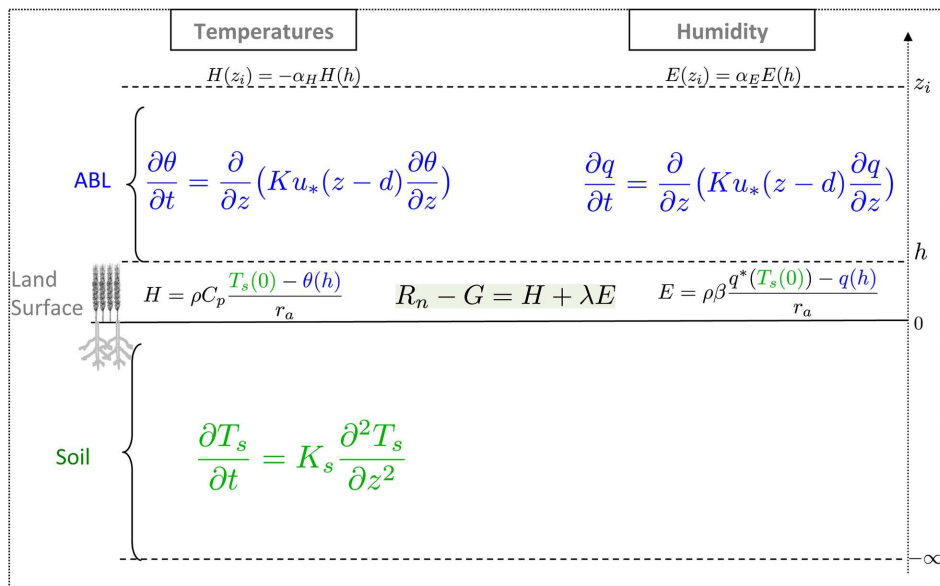


**Figure 1.** Schematic of the soil–vegetation–atmospheric boundary layer continuum model with the governing equations in each domain [*Gentine et al.*, 2010]. The coupling between the subsurface and the atmospheric boundary layer occurs at the surface through the turbulent heat fluxes  $H$  and  $\lambda E$ .

$R^2$  statistic was 89%. The soil properties are summarized in Tables 1 and 2.

### 2.3. SUDMED Augmented Data Set With a Land Surface Model

[20] To enhance the value of the observational data set we calibrate a high-resolution numerical model with the existing SUDMED field campaign observations. The numerical model parameters are adjusted in order to achieve the closest match between the states and fluxes at nodes where SUDMED observations are available. The numerical model is a high-resolution Soil Vegetation Atmosphere Transfer (SVAT) scheme and it is used to produce this enhanced data set (referred hereafter as the augmented data set). The calibrated numerical model provides the means to analyze positions in the profile that are not (or cannot) be observed. For example the temperature and flux profiles millimeters below the surface are difficult to measure over a long period of time where there is significant vegetation phenology or where there is soil disturbance due to human and animal impacts. Finally, the numerical model fills in temporal gaps in the records, thus allowing temporal spectral analysis.

[21] The choice of SVAT model is the Interactive Canopy Radiative Exchange (ICARE) model from the Centre d'Etudes Spatiales de la Biosphere (CESBIO), Centre National d'Etudes Spatiales (CNES). The soil heat flux is based on the multilayer version of ISBA [Habets *et al.*, 2003], the land surface model operationally used at Météo France. The soil heat transport includes both sensible and latent heat [Heitman *et al.*, 2008a, 2008b, 2010; Sakai *et al.*, 2011]. The inclusion of the latent heat flux within the soil profile is important since the simpler analytical model does not include this effect. In the numerical model the soil heat conservation is

$$C_h \frac{\partial T_s}{\partial t} = \frac{\partial G}{\partial z} + \Phi = \frac{\partial}{\partial z} \left( \lambda_g \frac{\partial T_s}{\partial z} \right) + \Phi, \quad (4)$$

where  $T_s$  is the soil temperature,  $C_h$  is the heat capacity,  $\lambda_g$  is the thermal conductivity, and  $\Phi$  is the soil water vapor latent heat flux, which depends on time and depth.

[22] We use a very fine discretization near the top of the soil. High vertical resolution is required to accurately resolve the heat transfer near the surface [Sakai *et al.*, 2011]. The heat scheme is discretized using 1 mm thick layers in the first 5 cm. The discretization changes to 1 cm resolution until 20 cm. Further in the subsurface the resolution changes to 10 cm and extends to the bottom of the soil profile located at 6 m below the surface. At this far-field depth the heat flux is assumed to be zero. The soil properties are nonuniform and are based on the observed soil

**Table 1.** Granulometric Soil Properties for SUDMED Field Site

Depth (cm)	Clay Fraction (%)	Sand Fraction (%)	Silt Fraction (%)	Organic Matter Fraction (%)
10	34.1	30.04	35.86	1.57
20	36.58	30.58	32.83	1.24
30	39.22	29.67	31.11	1.24
40	38.47	27.80	32.83	1.17
50	38.63	23.54	37.83	0.91

**Table 2.** Soil Heat and Hydraulic Properties for SUDMED Soils Based on Laboratory Testing

Variable	Value and Units
Potential at saturation	$\psi_{sat} = -0.3$ m
Shape parameter <sup>a</sup>	$B = 5.25$
Soil water content at saturation	$w_{sat} = 0.47$ m <sup>3</sup> m <sup>-3</sup>
Soil water content at field capacity	$w_{fc} = 0.379$ m <sup>3</sup> m <sup>-3</sup>
Soil water content at wilting point	$w_{wilt} = 0.14$ m <sup>3</sup> m <sup>-3</sup>
Soil dry density	$1.55 \times 10^3$ kg m <sup>-3</sup>
Soil dry specific heat	$900$ J kg <sup>-1</sup> K <sup>-1</sup>
Dry thermal conductivity	$0.75$ W m <sup>-1</sup> K <sup>-1</sup>
Hydraulic conductivity at saturation	$k_{sat} = 1.25 \times 10^{-6}$ m s <sup>-1</sup>

<sup>a</sup>Brooks and Corey [1964].

composition throughout the soil horizon (see Tables 1 and 2).

[23] The model is calibrated against the SUDMED observations (at matching positions and times) by minimizing the normalized  $R^2$  statistics with all the observed heat fluxes, soil moisture and surface infrared temperatures (at nadir and 55°) measurements during both the bare soil and vegetated periods [Gentine *et al.*, 2007]. The bare soil calibration allows estimation of the soil evaporation resistance. Accurate soil resistance is required for reliable energy and moisture partitioning between vegetated and soil fractions. Table 3 shows the root-mean-square error and  $R^2$  statistics between the calibrated ICARE SVAT time series and the field observations of net radiation ( $R_n$ ), latent heat flux ( $\lambda E$ ), sensible heat flux ( $H$ ), soil heat flux at 1, 10, and 30 cm below the surface ( $G_{1cm}$ ,  $G_{10cm}$ , and  $G_{30cm}$ , respectively).

## 3. Results

### 3.1. Surface Energy Budget Components

[24] Figure 2 shows the comparison of the gain amplitude and phase spectra between augmented observations and the analytical model, as a function of the period  $T$  (reciprocal of frequency  $\omega$ ) and with respect to incoming radiation forcing  $I_1$ . Both turbulent and radiative heat fluxes have a relatively amplified gain at longer periods  $T$  (lower frequencies) as shown in Figure 2 (top). The frequency response of sensible soil heat flux at the surface is the inverse of that for turbulent and radiative heat fluxes. The

**Table 3.** Statistics (Mean Value  $\bar{X}$ , Root-Mean-Square Error (RMSE), and Coefficient of Determination  $R^2$ ) of the Calibrated SVAT Outputs Against Measurements From the SUDMED Field Observations at a 30 min Resolution, Averaged Over the 101 Days of Gap-Free Measurements<sup>a</sup>

$X$	$\bar{X}$ (W m <sup>-2</sup> )	RMSE (W m <sup>-2</sup> )	$R^2$
$R_n$	106.9	28.6	0.98
$H$	31.4	44.3	0.82
$\lambda E$	93.1	47.6	0.85
$G_{1cm}$ , sensor 1	1.75	31.1	0.85
$G_{1cm}$ , sensor 2	-0.17	34.2	0.87
$G_{1cm}$ , sensor 3	0.91	26.9	0.89
$G_{10cm}$ , sensor 1	-0.74	8.8	0.88
$G_{10cm}$ , sensor 2	0.64	15.1	0.83
$G_{30cm}$	-0.93	4.1	0.85

<sup>a</sup>The statistics are calculated for net radiation  $R_n$  (daytime), sensible heat flux  $H$  (nonnegative values only), latent heat flux  $\lambda E$  (daytime), and soil heat flux  $G_z$  at different depths:  $z = 1, 10, \text{ and } 30$  cm (entire day).

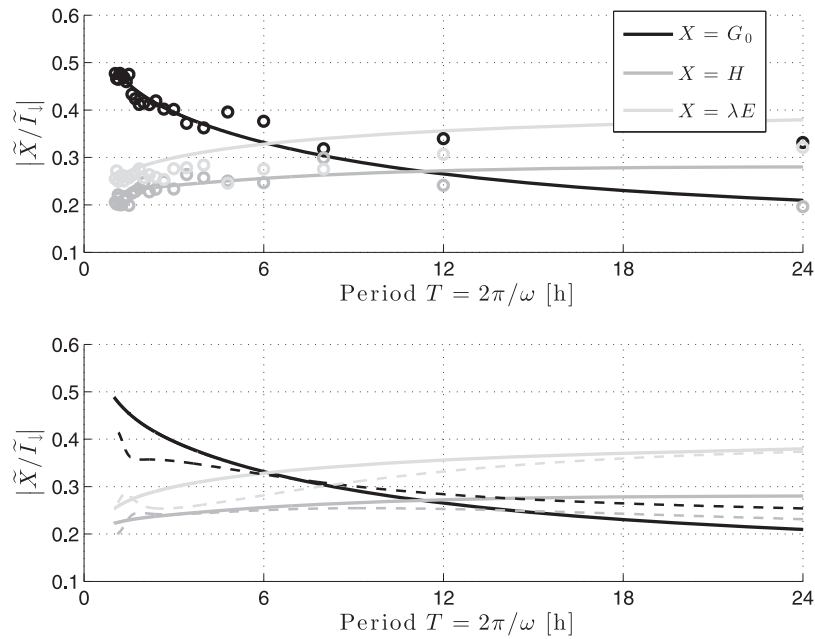


**Figure 2.** Comparison between the harmonics of surface heat fluxes  $G_0$  as the difference between net radiation and turbulent heat fluxes: surface soil, sensible ( $H$ ) and latent ( $\lambda E$ ) heat fluxes from the theoretical model (solid lines) with 66 days of continuous observations of the SUDMED project, as a function of the period  $T = 2\pi/\omega$ . (top) Comparison with mean observed spectrum averaged across days (i.e., the power spectrum of each flux is averaged at each daily frequency across all measurement days). The high frequencies are well captured by the theoretical model. (bottom) The same plot, but using a Yule-Walker filter of the observations (dashed line), which is more representative of the lower-frequency component by construct. This lower-frequency component is well reproduced by the theoretical model (similar to Figure 2 of Gentine *et al.* [2011]).

amplitude response of soil heat flux is higher at shorter periods  $T$ , i.e., at high frequencies. Surface soil heat flux acts as a high-pass filter of incoming radiation. This result was demonstrated theoretically by Gentine *et al.* [2010, 2011] and corroborated by the experimental observations of Heusinkveld *et al.* [2004].

[25] This result has important implications for the characterization of the surface heat fluxes in models and for in situ observations of the surface energy balance. The coupling of the soil and atmospheric media introduces new time scales at the surface. The high frequencies ( $T \leq 6$  h) of incoming radiation are preferably amplified in the surface soil heat flux component and the low frequencies mostly dissipate through turbulent heat fluxes to the atmosphere. Since heat dissipation in the soil is slow, high frequencies remain concentrated in a very shallow surface soil layer. This results in steep temperature gradients in the near-surface soil. The sensible soil heat flux responds to these steep surface gradients [Gentine *et al.*, 2011].

[26] The incoming radiation spectrum is shown on Figure 3 for a typical clear sky and cloudy day. The clear-sky spectrum only displays two main daily harmonics at  $T = 12$  and 24 h. The radiation spectrum of the cloudy day exhibits a much broader spectrum with many frequencies below 12 h, induced by the variables cloudiness. The high frequencies due to intermittent clouds are preferentially dissipated as soil heat flux. Incorrect measurements of the soil heat flux high frequencies can introduce artificial low-pass filter  $F_{G_0}(G_0)$ , introducing

energy closure errors by distortion of the original frequency spectrum.

### 3.2. Sensible Soil Heat Flux Profile

#### 3.2.1. Frequency Response

[27] The soil-vegetation-ABL continuum model can be used to map the spectral gain and phase of the soil heat flux at a continuum of depths. Advantageously and in contrast to numerical models, the continuum model estimation of spectral response is not constrained by the Nyquist frequency.

[28] Figure 4 shows the analytical ratio of the amplitude (gain) of soil heat flux at depth  $G(z)$  with respect to the value at the surface  $G_0$  as a function of the period  $T$ . At the surface, sensible soil heat flux absorbs the high frequencies that may be present in intermittent (e.g., cloudy) incoming radiation. The analytical model shows that the high-frequency component is rapidly attenuated throughout the soil profile [Horton and Wierenga, 1983a; Horton *et al.*, 1983; Wang *et al.*, 2010]. At 5 cm below the surface, the soil heat flux is virtually insensitive to the high-frequency components of surface soil heat flux  $G_0$ . Even at 1 cm more than 50% of the surface signal is lost. Near-surface (0–1 cm) measurements are required to accurately estimate soil surface sensible heat flux.

[29] Figure 5 shows the phase spectrum between the soil heat flux at depth,  $G(z)$ , and the surface soil heat flux,  $G_0$ . The phase spectrum is also a function of depth and period  $T$  of the signal. At high periods  $T$  or low daily frequencies,

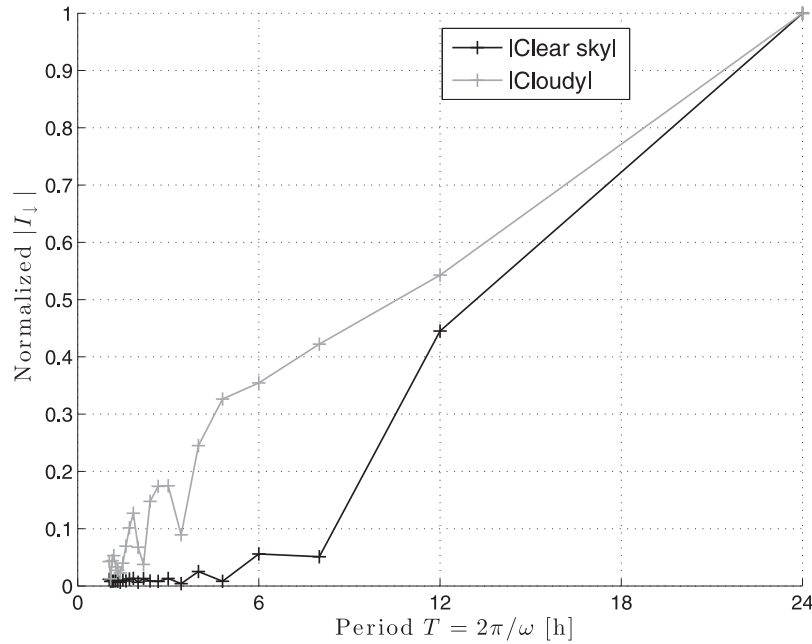


**Figure 3.** Comparison of the observed incoming radiation spectrum based on the SUDMED data set on DOY 83 (clear sky) and DOY 92 (cloudy). In the clear-sky case, only the main daily harmonics (24 and 12 h) are present in the incoming radiation spectrum. During the cloudy day, the incoming radiation spectrum is broader and contains power in frequencies below the 12 h period.

the temporal lag between the soil heat flux at the surface and at 5 cm is about 2 h. At the short period  $T = 30$  min to 1 h (typical averaging period for field measurements and time step of most operational SVATs), the phase lag is about 15–30 min at 5 cm and 7–15 min at 2 cm. Soil heat flux deeper in the soil lags the surface signal significantly

and is a poor indicator of the instantaneous surface soil heat flux.

[30] There is a fundamental phase difference between the soil heat flux measured or modeled at some depth  $z$  and that at the surface. Any measurements of deeper soil heat flux have to be corrected for time lag in order to be brought

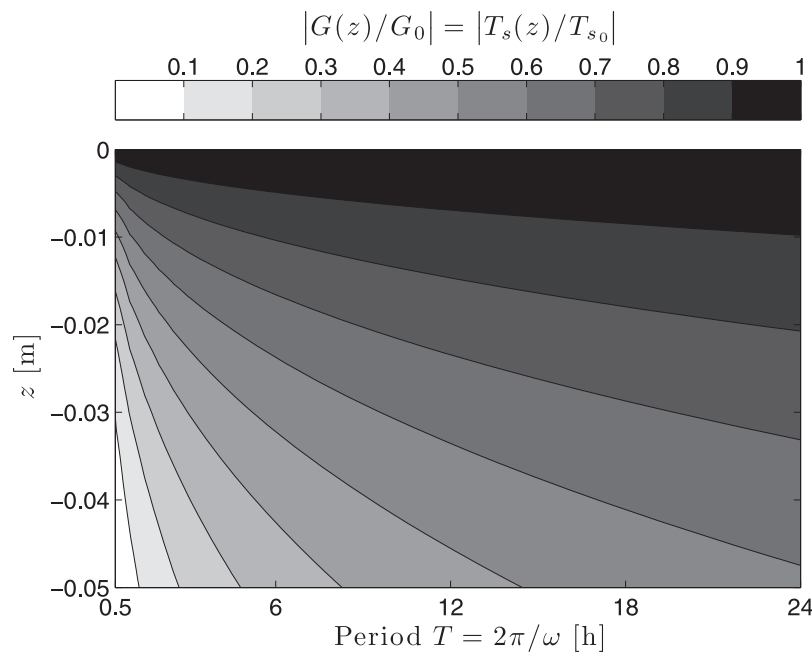


**Figure 4.** Contours of the amplitude attenuation of soil heat flux as a function of depth  $z$  and period  $T$  relative to the value at the surface  $G_0$ .



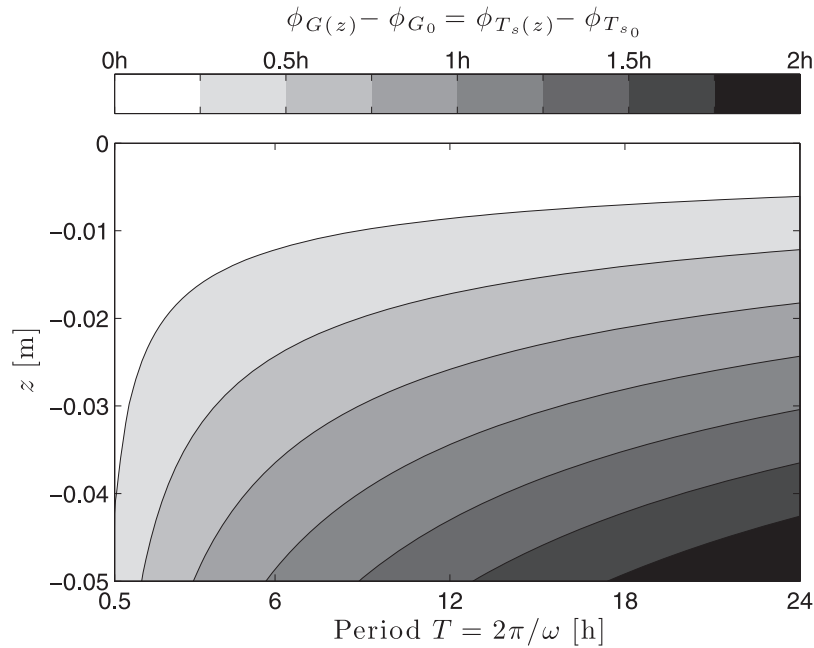


**Figure 5.** Contours of the phase of soil heat flux as a function of depth  $z$  and period  $T$  relative to the value at the surface  $G_0$ , expressed in hours.

into phase agreement with  $G_0$ . This is widely recognized and the subject of many attempts at empirical corrections for the phase errors [Gao *et al.*, 2010; Wang and Bou-Zeid, 2011].

[31] The analytical model does not take into account variations in soil thermal properties and soil latent heat flux. The SVAT model takes into account the latent heat transport as well as the soil moisture and water vapor dynamics throughout the soil horizon. Soil thermal properties (specific heat content, thermal diffusivity) are nonlinear functions of soil water content. A sensitivity test is necessary because the analytical solution for the soil-vegetation-ABL continuum model relies on an effective (fixed) value of soil thermal properties and models only sensible heat dissipation.

[32] The gain spectra of soil heat flux at 5 cm with respect to the surface soil heat flux is a compact measure of how much soil moisture affects the penetration depth of soil temperature waves across this layer. Figure 6 tests the impact of soil water content (both constant and dynamic) on soil heat flux at the surface and 5 cm below the surface along with the effect of incorporating latent heat of water vapor. Numerical experiments using the calibrated SVAT show that the gain spectra are similar across the dynamic range of moisture conditions. The inclusion of latent heat flux within the soil profile does not modify the conclusions reached using the theoretical model. Furthermore the results are insensitive to the nonuniformity of the soil heat properties: linearly increasing dry bulk density by 50% throughout the first meter of the soil profile (or using observed profiles) has negligible impacts on the results (not shown).

### 3.2.2. Correlation With Surface Heat Flux

[33] Figure 7 shows the correspondence between soil heat flux at depths 1, 2.5, 5, and 10 cm below the surface and the surface soil heat flux value computed as the residual  $G_0 = R_n - H - \lambda E$ , using the augmented data set

(SUDMED observations and the SVAT model). The instantaneous correlation captures the errors induced by the amplitude and phase differences. Soil heat flux at 1 cm below the surface is well correlated with the surface value (Figure 7a) since it captures the high-frequency components of the surface and since the phase delay with the surface heat flux is relatively small. It nonetheless underestimates the amplitude of  $G_0$  by about  $13 \text{ W m}^{-2}$  on average (departure from the 1:1 line). This error contributes to closure error in the surface energy budget.

[34] The underestimation of the surface soil heat flux is large using depths as shallow as 2.5 cm (Figure 7b). The correlation is diminished to 0.95 and scatter increases. The reduction in the correlation can be attributed to the attenuation of the high frequencies and introduction of a larger temporal lag with the surface. Correlation captures the correspondence in phase and hence it is sensitive to lag differences in the series. On average the soil heat flux at 2.5 cm is underestimating  $G_0$  by about  $31 \text{ W m}^{-2}$ . These errors would propagate to the surface energy balance if used without care and correction. Correlation reduces deeper into the soil profile. Figures 7c and 7d show that the correlations are reduced to 0.81 and 0.38 at 5 and 10 cm below the surface, respectively. These are typical depths at which soil heat flux plates are installed. Figures 7c and 7d also show that soil heat fluxes at 5 and 10 cm strongly underestimate the surface soil heat flux value, when compared to the 1:1 line. The underestimation is on average  $66 \text{ W m}^{-2}$  at 5 cm. At 10 cm the signal appears uncorrelated with the surface value. The surface energy balance errors induced by using the direct soil heat flux at 1, 2.5, 5, and 10 cm in lieu of  $G_0$  are respectively 14, 30, 50, and  $73 \text{ W m}^{-2}$ . These errors are important contributors to the apparent lack of closure of the surface energy balance using independent observations (see section 5). The amount of the error contribution is a function of temporal frequency as shown in this study.

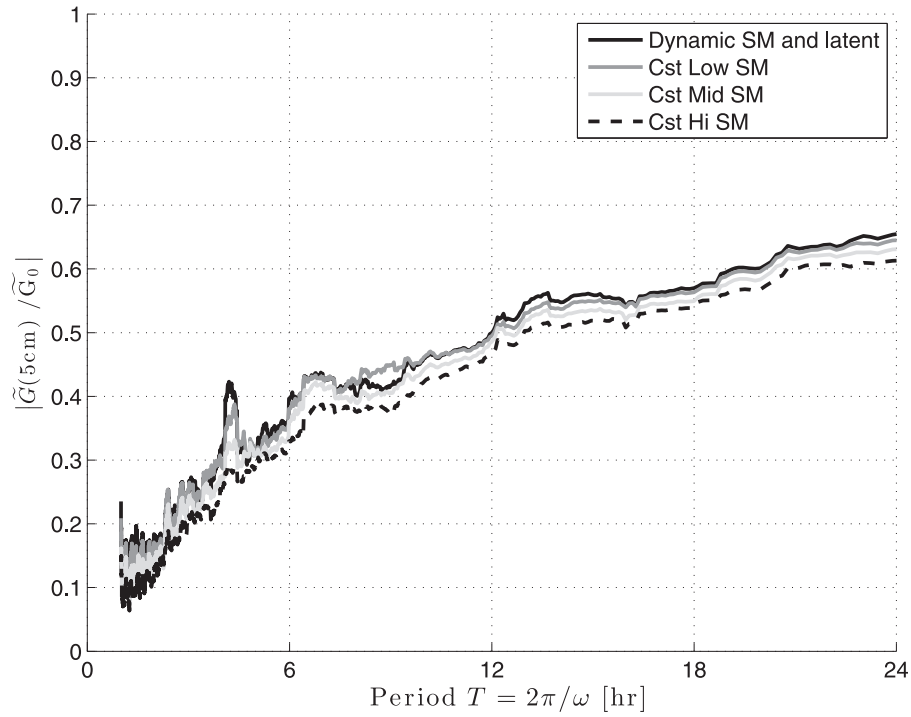


**Figure 6.** Impact of soil moisture on the frequency response of the amplitude of soil heat flux at 5 cm relative to the value at the surface. In the dynamic case, soil moisture is allowed to vary with time, and it includes water vapor latent heat flux. Also shown are experiments where soil moisture is held constant at  $w_{wilt} + 1/3(w_{fc} - w_{wilt}) = 0.225 \text{ m}^3 \text{ m}^{-3}$  for the low soil moisture case,  $w_{wilt} + 2/3(w_{fc} - w_{wilt}) = 0.3 \text{ m}^3 \text{ m}^{-3}$  for the medium soil moisture case, and  $w_{fc} = 0.379 \text{ m}^3 \text{ m}^{-3}$  for the high soil moisture case.

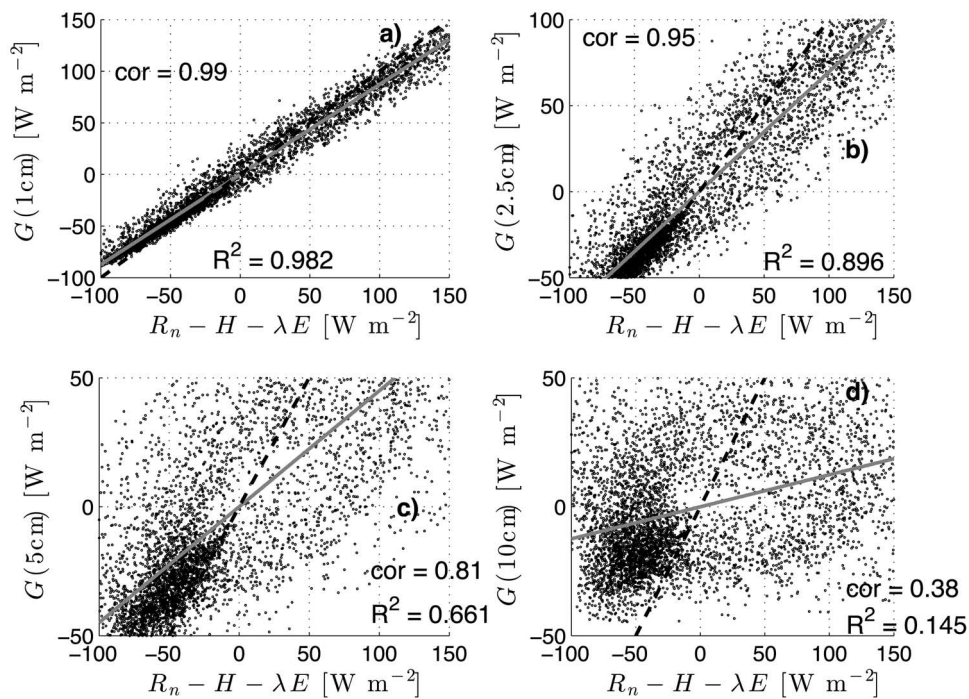


**Figure 7.** Correspondence of soil heat flux at (a) 1, (b) 2.5, (c) 5, and (d) 10 cm with surface soil heat flux  $G_0 = R_n - H - \lambda E$ . The gray line represents regression line using 30 min resolution outputs of the SVAT model (augmented data set). The dashed line represents the 1:1 line. Explained variance and correlation values are also shown for each panel.



#### 4. Temporal Averaging Effect

[35] The soil-vegetation-ABL continuum model and its spectral solution can be used to illustrate another type of error that can potentially affect energy balance closure, especially under partially cloudy conditions. Here we use a truncated Fast Fourier Transform of the soil heat flux at the surface in the augmented data set to evaluate the effect of a coarser temporal resolution.

[36] A schematic of the effect of time averaging soil heat flux data and surface energy balance is shown in Figure 8. Time averaging introduces a step transfer function in the frequency domain and thus a low-pass filter  $F_X$ . Truncation occurs at the Nyquist frequency (half of the sampling frequency). This filter or transfer function  $F_X$  applies to the components of the surface energy balance (Figure 2, top). Clearly the surface soil heat flux is the component that is most affected because it absorbs most of the high-frequency fluctuations that fall in the opaque spectral portion of the transfer function. The spectral power or amount of fluctuations at high frequencies (minutes and up to hours) is relatively small compared to the principal diurnal cycle. Features outside of the diurnal cycle are nonetheless important to the surface energy balance and to reducing its closure errors.

[37] Figure 9, based on 1 day of observations at the SUDMED site, provides an example of the effects in time rather than in frequency. During this sample day a cloud passes over the site around noon. This leads to a sharp drop in solar incoming radiation. There is a corresponding drop in the soil heat flux that has 30 min (native) temporal resolution. For longer temporal averaging periods, the sharp drop in the surface soil heat flux is not evident because it is attenuated by the time-averaging filter. The surface energy balance closure is affected by such mismatches in the spectral characteristics of the different measurements. The error in the surface soil heat flux is significant since the more

filtered soil heat fluxes are missing about half of the signal, i.e.,  $60 \text{ W m}^{-2}$ .

#### 5. Existing Approaches for Inferring $G_0$ From $G(z)$ : Calorimetric Method

##### 5.1. Typical Estimation Strategy

[38] Corrections such as a Fourier reconstitution of the surface soil heat flux value from deeper measurements have been traditionally used to infer  $G_0$  [deSilans *et al.*, 1997; Heusinkveld *et al.*, 2004; Wang and Bou-Zeid, 2012]. Temperature measurements deeper in the soil are also used for correction [Horton and Wierenga, 1983a; Wang and Bras, 1999]. These methods use several daily harmonics or temporal variations of observed temperature and soil heat flux at depth to reconstruct surface soil heat flux.

[39] Methods have also been developed to use temperature measurement time series to infer soil heat flux. These methods include Harmonic analysis [Horton and Wierenga, 1983a], Green's function methods [Wang and Bras, 1999; Wang and Bou-Zeid, 2012] or empirical method that include water vapor effects near the surface [Holmes *et al.*, 2008]. The advantage of those methods is that a temperature probe can be buried in the topsoil at about 1 cm, whereas soil heat flux plate installation at this depth is much more complicated. The recent development of new, heated, sensors, such as the three-needle gradient [Ochsner *et al.*, 2006] or active distributed temperature sensing (DTS) [Sayde *et al.*, 2010], provide an improved framework for estimating both the near-surface temperature and the soil heat conductivity.

[40] Perhaps the most common method to infer  $G_0$  is the calorimetric approach. In this approach one or several soil temperature probes (temperature sensor or pulse heat probe) are buried between the surface and the heat flux plate, located at depth  $\Delta z$ . The heat flux plate is usually buried at

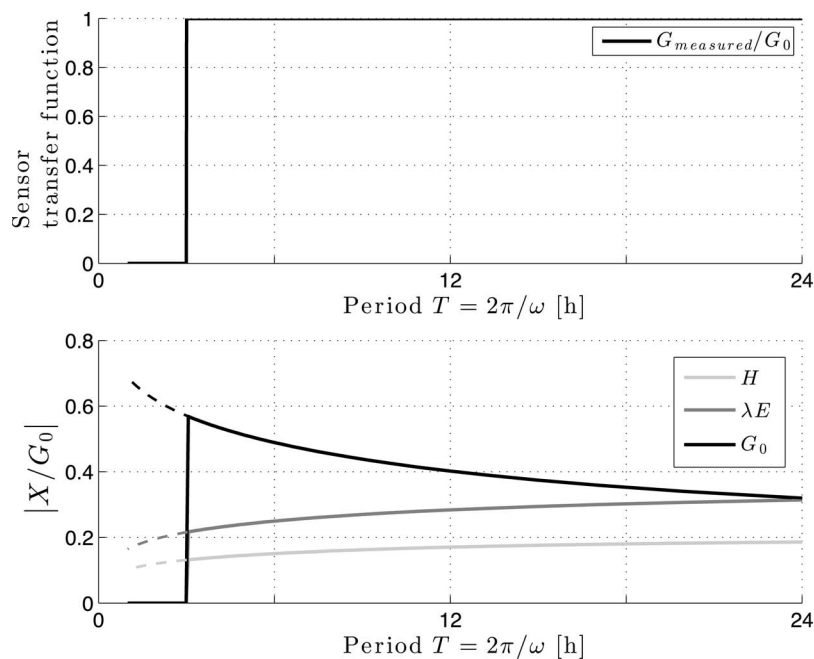


**Figure 8.** (top) The effects of time averaging on surface soil heat flux as a spectral filter. (bottom) The effects of time averaging on the components of surface energy balance as a function of frequency.

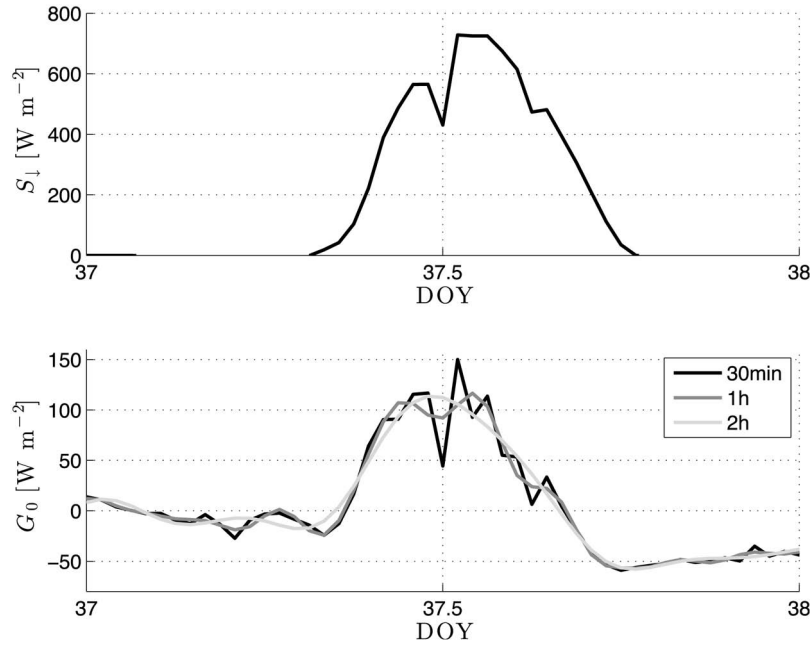


**Figure 9.** Example of the impact of the passage of intermittent clouds on soil heat flux depending on the temporal averaging period (SUDMED observations)

5 to 20 cm below the surface. According to the calorimetric method, the surface soil heat flux is the sum of the heat flux at depth plus the time rate of change in the heat content of the intervening layer. *Massman* [1993] discusses in detail the weights needed to be applied to the temperature probe data in order to obtain reliable surface soil heat flux. Here we show how an inconsistent temperature measurement location can artificially modulate the retrieved surface soil heat flux spectrum.

[41] In the calorimetric method the temperature probes at shallower depth are used to evaluate the variations of the storage term and latent heat storage is neglected [*Ochsner et al.*, 2007]. The soil temperature is assumed uniform between probes. Then it is relatively straightforward to evaluate the derivative of the storage term with an assumed heat capacity of the soil  $C_h$ . In the case of a single probe (easily generalizable to several probes) with assumed uniform soil heat capacity, the storage variations are related to the temperature variations as

$$\frac{dS}{dt} = C_h \frac{dT_s(\Delta z_0)}{dt} \Delta z, \quad (5)$$

where  $S = C_h \int_0^{\Delta z} T_s dz$  is the heat storage above the soil heat flux plate depth.

[42] This heat storage change is considered to be equal to the divergence of ground heat flux between the surface and  $\Delta z$ :

$$C_h \frac{dT_s(\Delta z_0)}{dt} \Delta z = G_0 - G_{\Delta z}. \quad (6)$$

The energy conservation (6) and the estimate of heat storage change (5) provide for the basis for the calorimetric method approach to the estimation of  $G_0$ . The temporal derivative is proportional to frequency in the Fourier domain. The change in the storage term is large at the highest frequencies. The

sensible soil heat flux at depth has less power in high frequencies. Therefore the high frequencies of the surface soil heat flux are mostly present in the storage term.

## 5.2. Systematic Errors Introduced by Calorimetric Measurement Methodology: Measurement Depths

[43] Here we focus on the typical application of the calorimetric method with a single temperature but the argument is valid for multiple temperature probes as well. Figure 10 shows the statistical regression between the 30 min surface soil heat flux  $G_0$  (as the difference between  $R_n$  and  $H + \lambda E$ ) and the reconstructed surface soil heat flux using the calorimetric method. The augmented data set is used here. Two soil heat flux measurement depths are used for the calorimetric method application examples: 5 and 10 cm with intermediate soil temperature measurements (i.e., 2.5 and 5 cm). The calorimetric method yields relatively good  $R^2$  statistics since the diurnal cycle is dominant. Closer inspection of the closure errors show that the calorimetric method has Root Mean Square Errors of  $13 \text{ W m}^{-2}$  using soil heat flux plate at 5 cm and temperature correction at 2.5 cm and  $23 \text{ W m}^{-2}$  using soil heat flux plate at 10 cm and temperature correction at 5 cm. In addition the maximum absolute error is  $123 \text{ W m}^{-2}$  with 5 cm soil heat flux and  $201 \text{ W m}^{-2}$  with 10 cm soil heat flux. The maximum error is of the order of the soil heat flux amplitude.

[44] The calorimetric method is based on the assumption that the measurements of soil temperature at some depth  $\Delta z_0$  above the soil heat flux plate approximate the heat storage above the soil heat flux plate. Mathematically, this means that the soil temperature depth is chosen so that (assuming a constant soil heat capacity)

$$\frac{d}{dt} \int_0^{\Delta z} T_s(z) dz \approx \frac{dT_s(\Delta z_0)}{dt} \Delta z. \quad (7)$$

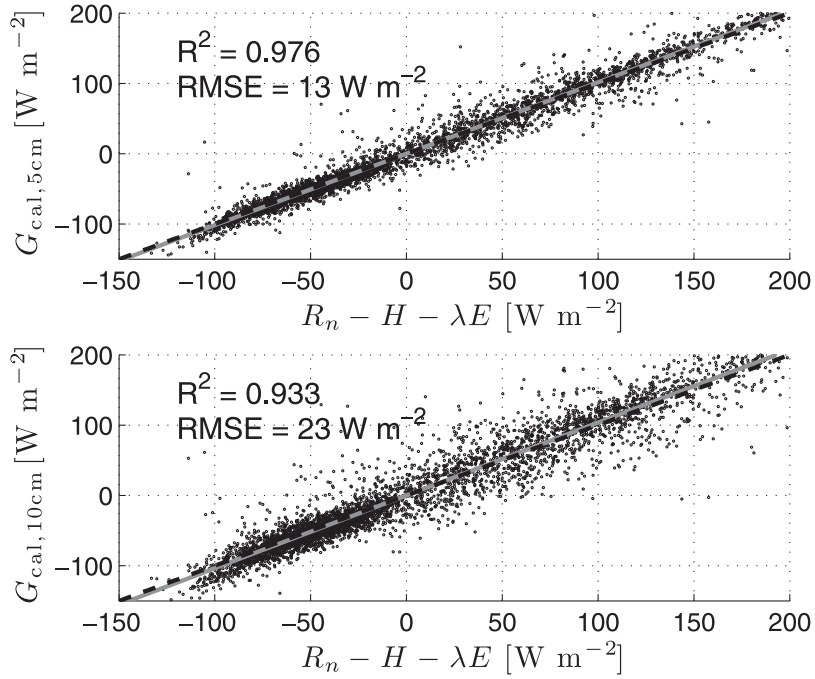


**Figure 10.** Scatter plots of the 30 min soil heat flux at the surface  $G_0$  and the reconstructed calorimetric method with (top) the soil temperature at 2.5 cm and heat flux at 5 cm and (bottom) the soil temperature at 5 cm and heat flux at 10 cm, using the augmented data. The gray line represents regression line. The dashed line represents the 1:1 line.

In complex notation the soil temperature field can be written as sum of harmonics:

$$T_s(z) = \bar{T} + \sum_{n=-M, n \neq 0}^M \widetilde{T}_{\Delta z_0, n} \exp(j\omega_n t) \exp\left(- (1+j) \frac{z - \Delta z_0}{l(n)}\right), \quad (8)$$

where  $l(n) = \sqrt{2D_h/n\omega_0}$  is the penetration depth at daily harmonic number  $n$  and  $\widetilde{T}_{\Delta z_0, n}$  represents the complex amplitude of soil temperature at depth  $\Delta z_0$ ,  $T_s(\Delta z_0)$ , and at daily harmonic number  $n$  [Carslaw and Jaeger, 1959]. A Taylor expansion of this expression around  $\Delta z_0$  gives

$$T_s(z) = \bar{T} + \sum_{n=-M, n \neq 0}^M \widetilde{T}_{\Delta z_0, n} \exp(j\omega_n t) \left(1 - (1+j) \frac{z - \Delta z_0}{l(n)} + O\left(\frac{z - \Delta z_0}{l(n)}\right)^2\right). \quad (9)$$

The integral term in (7) can be rewritten as

$$\int_0^{\Delta z} T_s(z) dz = \bar{T} \Delta z + \sum_{n=-M, n \neq 0}^M \widetilde{T}_{\Delta z_0, n} \exp(j\omega_n t) \left(\Delta z + \frac{1+j}{l(n)} \Delta z \left(\Delta z_0 - \frac{\Delta z}{2}\right) + O\left(\frac{\Delta z - \Delta z_0}{l(n)}\right)^3\right). \quad (10)$$

[45] The approximation in (7) can only hold if the imaginary part on the right-hand side vanishes. This imposes the choice of  $\Delta z_0 = \Delta z/2$  in the case of a single temperature

probe. Using this measurement depth (the daily mean term drops out when applying the time derivative),

$$\frac{d}{dt} \int_0^{\Delta z} T_s(z) dz = \Delta z \frac{d}{dt} \left( \sum_{n=-M, n \neq 0}^M \widetilde{T}_{\Delta z_0, n} \exp(j\omega_n t) + O\left(\frac{\Delta z}{2l(n)}\right)^3 \right). \quad (11)$$

This shows that using the midpoint temperature measurements the surface soil heat flux spectrum can hypothetically be reconstructed since no harmonics appear in (11) except in the  $O\left(\frac{\Delta z}{2l(n)}\right)^3$  term. At other depths reconstruction of the surface soil heat flux would be distorted without harmonic correction [Massman, 1993].

[46] Figure 10 shows that this reconstruction is still lossy and that it contributes to the lack of surface energy balance closure. Figure 11 further demonstrates the errors introduced by different combinations of soil heat flux plate and soil thermistor instrument installation positions. Figure 11 is based on the continuum model with a temperature probe located at different depths and with a soil heat flux measurement evaluated at 5 cm. When soil heat flux plate is buried too deep (more than half distance to the surface), it is not possible to fully reproduce the surface soil heat flux spectrum with the calorimetric method, especially at high frequencies. This is due to the breakdown of the linearity assumption in (11).

[47] The major issue with the calorimetric methodology is that the accuracy depends on the magnitude of the  $O\left(\frac{\Delta z}{2l(n)}\right)^3$  term. At low frequencies  $l(n)$  is of the order of a few tens of centimeters. Therefore the main diurnal harmonics are reconstructed well. At higher frequencies ( $T = 1$  h),

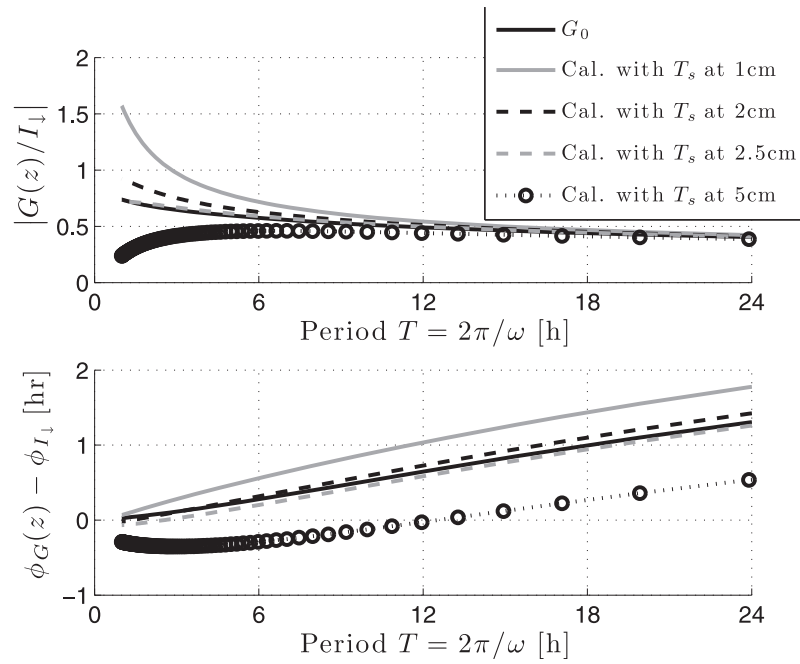


**Figure 11.** Theoretical reconstruction of surface soil heat flux  $G_0$  from the calorimetric method with a soil heat flux plate at 5 cm and soil temperature evaluated at different depths.

$l(n)$  becomes small, of the order of 1 cm. Subsequently to avoid any deformation of the reconstructed surface soil heat flux spectrum, the first temperature probe should ideally be located less than 1 cm below the surface. In the case of a single probe this is unrealistic since the soil heat flux plate would have to be located at about 2 cm below the surface.

[48] The methodology can be extended to several temperature probes such as performed by *Horton and Wierenga* [1983b] and *Massman* [1993]. In the case of two (three) probes, the temperature probes would have to be located at depths  $\Delta z/4$  and  $3\Delta z/4$  ( $\Delta z/6$ ,  $\Delta z/2$ , and  $5\Delta z/6$ ) to avoid spectral distortion of the surface heat flux.

## 6. Temporal Aliasing

[49] There is an aliasing effect introduced by the discretized time derivative of soil temperature that is used to estimate the heat storage term. In most applications of the calorimetric method the temperature derivative, representing the heat storage term, is approximated with a numerical difference applied to the time series. This introduces an artificial low-pass filter of soil heat flux  $F_{G_0}(G_0)$ . For instance, a first-order derivative can be evaluated with the time series as  $(x_{n+1} - x_n)/\Delta t$ , with  $\Delta t$  as the time step between measurements. In the (discrete) Fourier domain this gradient corresponds to a phase shift  $\exp(j2\pi k/N) - 1$  or  $\exp(j\omega) - 1$  at harmonic number  $k$  (an increment in time corresponds to a phase shift in the Fourier domain). Based on Fourier derivative, the accurate time derivative in the frequency domain should be a  $j2\pi k/N$  or  $j\omega$  factor.

[50] The transfer functions for both temporal derivative transfer functions are shown in Figure 12. The numerical time series derivatives  $(x_{n+1} - x_n)/\Delta t$ , i.e.,  $\exp(j2\pi k/N) - 1$  in the Fourier domain, underestimates the high-frequency spectrum. This also holds true for more complicated derivative such as a the center point method. Figure 13 confirms that the

usual calorimetric method, which evaluate the derivative as  $\Delta T_s/\Delta t$ , does not reconstruct the high-frequency components of the surface soil heat flux. In contrast, we can reconstruct the original high-frequency spectrum by multiplying the numerical derivative by  $j2\pi k/N/(\exp(j2\pi k/N) - 1)$  in the frequency domain. This reconstructed spectrum does reproduce the high-frequency portion of the surface spectrum as shown in Figure 13.

[51] Based on tests with the SUDMED augmented data set, the reconstructed spectrum using the derivative correction leads to a reduction of errors in estimated  $G_0$  using the calorimetric method. Using the calorimetric method with soil heat flux plate at 5 cm below the surface and a temperature probe at 2.5 cm below the surface resulted in an RMSE of  $13 \text{ W m}^{-2}$  and a maximum absolute error of  $123 \text{ W m}^{-2}$  (the differences are between the calorimetric method estimation  $G_0$  and  $R_n - \lambda E - H$ ). When the correction methodology proposed above is applied, the RMSE is reduced to  $7 \text{ W m}^{-2}$  (almost halved) and the maximum absolute error is reduced to  $82 \text{ W m}^{-2}$  (almost one-third reduction). The loss of high-frequency information is a problem that can be partially addressed in order to improve surface energy balance closure.

## 7. Conclusion

[52] In this study the role of temporal and subsurface positioning sampling of soil heat content and flux is investigated using field observations, a numerical model calibrated to field observations, and the solution of an analytical model of the soil–vegetation–atmospheric boundary layer continuum. The study focuses on the differences in the frequency dependence of the components of the surface energy balance. The coupling of the soil, characterized by slow time scales of heat dissipation, and of the atmosphere, characterized by rapid heat dissipation through turbulence, leads to

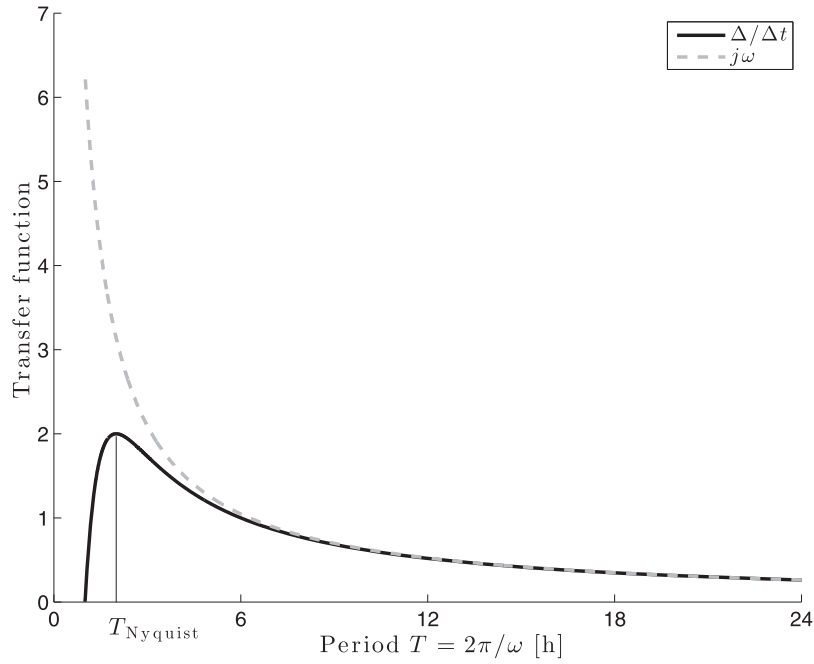


**Figure 12.** Transfer function of the time derivative evaluated as a finite difference in the temporal domain  $\exp(jn\omega) - 1$  (solid black line). The factor  $jn\omega$  in the frequency domain corresponds to the true time derivative.  $T_{\text{Nyquist}}$  depicts the Nyquist period, the inverse of the Nyquist frequency.

an opposite behavior at the interface. Surface soil heat flux concentrates the high-frequencies of incoming radiation since the heat flux can only slowly dissipate through the soil, whereas turbulent heat fluxes amplify longer time scale forcing. Furthermore the soil and the air media are capable

of maintaining different gradients of temperature that has its own influence on the surface energy balance components dynamics under different time scales of forcing fluctuations. [53] The main contribution of this study is the insight that surface soil heat flux absorbs the high frequencies

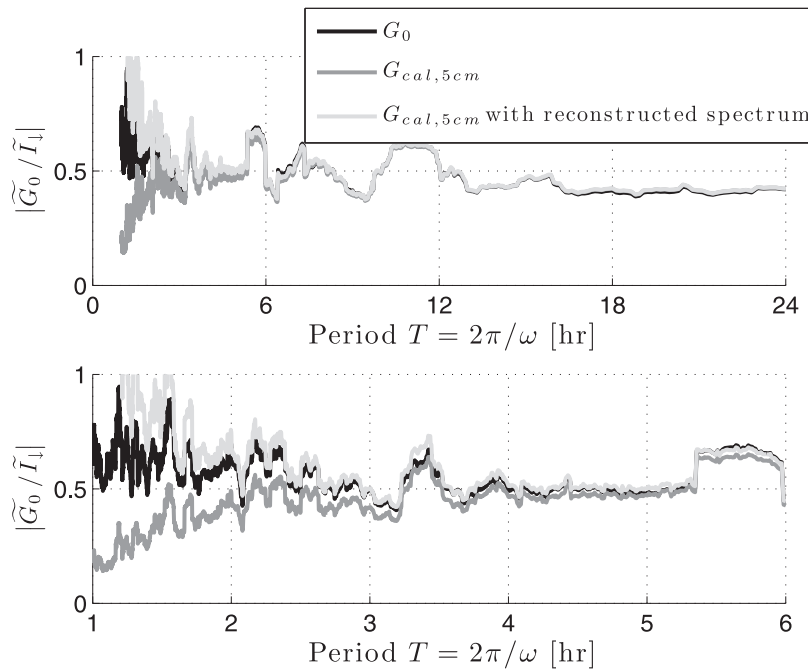


**Figure 13.** (top) Comparison of the spectrum of surface soil heat flux  $G_0$  (black line) with the calorimetric method evaluated with a typical numerical time derivative  $\Delta T_s / \Delta t$  (dark gray line) and with a corrected spectrum (multiplied by  $jn\omega / (\exp(jn\omega) - 1)$ ; light gray line), normalized by incoming radiation  $I_1$ . (bottom) Close-up of the high-frequency component.

(periods  $T \leq 6$  h) of incoming radiation. These high frequencies are strongly attenuated in amplitude and lagged in time (phase shift) at depth of even a few centimeters in the soil profile. Intermittent cloudiness thus strongly impacts soil sensible heat flux since it introduces high frequencies in the surface soil heat flux spectrum. In this study we show that most of the soil heat flux signal is located within the 0–1 cm layer. In situ measurements of soil heat flux should be made as close as possible to the surface and recorded at high frequency (1–5 min). Similarly, land surface models need at least 1 cm resolution near the surface to avoid distortion of the surface energy budget.

[54] The calorimetric method within a shallow soil profile has the potential to reconstruct well some of the richness of the high-frequency spectrum at the surface. This is so long as measurements are accurate and properly placed in the soil profile. The temperature probe (for single probe approach) needs to be positioned as close as possible to the surface (1 cm) to accurately observe the high-frequency components of the soil heat flux. We suggest burying a heat flux plate at  $\Delta z = 6$  cm and using three temperature probes at  $\Delta z/6 = 1$  cm,  $\Delta z/2 = 3$  cm and  $5\Delta z/6 = 5$  cm or use the *Horton and Wierenga* [1983b] approach of determining an average temperature for a soil layer. In addition, derivatives should be calculated on data stored at the higher temporal resolution (e.g., 5 min for aggregates at 30 min). With these field specifications the surface soil heat flux signal can be reconstructed with minimal distortion, especially at the highest frequencies.

[55] **Acknowledgments.** The authors would like to thank the SUDMED team for providing the data used in this paper. We also wish to thank seven anonymous reviewers and the editors for their valuable comments, which have helped improve the manuscript.

## References

- Baldocchi, D., B. Hicks, and T. Meyers (1988), Measuring biosphere-atmosphere exchanges of biologically related gases with micrometeorological methods, *Ecology*, *69*(5), 1331–1340.
- Beyrich, F., H. De Bruin, W. Meijninger, J. Schipper, and H. Lohse (2002), Results from one-year continuous operation of a large aperture scintillometer over a heterogeneous land surface, *Boundary Layer Meteorol.*, *105*(1), 85–97.
- Brooks, R., and A. Corey (1964), Hydraulic properties of porous media, *Hydrol. Pap. 3*, Colo. State Univ., Fort Collins.
- Carlsaw, H. S., and J. C. Jaeger (1959), *Conduction of Heat in Solids*, 510 pp., Oxford Univ. Press, Oxford, U. K.
- Chehbouni, A., et al. (2000), Estimation of heat and momentum fluxes over complex terrain using a large aperture scintillometer, *Agric. For. Meteorol.*, *105*(1–3), 215–226.
- Chehbouni, A., et al. (2008), An integrated modelling and remote sensing approach for hydrological study in arid and semi-arid regions: The SUDMED programme, *Int. J. Remote Sens.*, *29*(17–18), 5161–5181, doi:10.1080/01431160802036417.
- deSilans, A., B. Monteny, and J. Lhomme (1997), The correction of soil heat flux measurements to derive an accurate surface energy balance by the Bowen ratio method, *J. Hydrol.*, *189*(1–4), 453–465.
- Duchemin, B., et al. (2006), Monitoring wheat phenology and irrigation in central Morocco: On the use of relationships between evapotranspiration, crops coefficients, leaf area index and remotely-sensed vegetation indices, *Agric. Water Manage.*, *79*(1), 1–27.
- Eugster, W., J. McFadden, and E. Chapin (1997), A comparative approach to regional variation in surface fluxes using mobile eddy correlation towers, *Boundary Layer Meteorol.*, *85*(2), 293–307.
- Ezzahar, J., and A. Chehbouni (2009), The use of scintillometry for validating aggregation schemes over heterogeneous grids, *Agric. For. Meteorol.*, *149*(12), 2098–2109.
- Foken, T., and S. Oncley (1995), Workshop on instrumental and methodical problems of land-surface flux measurements, *Bull. Am. Meteorol. Soc.*, *76*(7), 1191–1193.
- Fuchs, M., and A. Hadas (1972), The heat flux density in a nonhomogeneous bare loessial soil, *Boundary Layer Meteorol.*, *3*, 191–200.
- Fuchs, M., and A. Hadas (1973), Analysis of performance of an improved soil heat-flux transducer, *Soil Sci. Soc. Am. J.*, *37*(2), 173–175.
- Gao, Z. (2005), Determination of soil heat flux in a Tibetan short-grass prairie, *Boundary Layer Meteorol.*, *114*(1), 165–178.
- Gao, Z., R. Horton, and H. P. Liu (2010), Impact of wave phase difference between soil surface heat flux and soil surface temperature on soil surface energy balance closure, *J. Geophys. Res.*, *115*, D16112, doi:10.1029/2009JD013278.
- Gentine, P., D. Entekhabi, A. Chehbouni, G. Boulet, and B. Duchemin (2007), Analysis of evaporative fraction diurnal behaviour, *Agric. For. Meteorol.*, *143*, 13–29.
- Gentine, P., D. Entekhabi, and J. Polcher (2010), Spectral behaviour of a coupled land-surface and boundary-layer system, *Boundary Layer Meteorol.*, *134*(1), 157–180.
- Gentine, P., J. Polcher, and D. Entekhabi (2011), Harmonic propagation of variability in surface energy balance within a coupled soil-vegetation-atmosphere system, *Water Resour. Res.*, *47*, W05525, doi:10.1029/2010WR009268.
- Green, E., and Y. Hayashi (1998), Use of the scintillometer technique over a rice paddy, *Jpn. J. Agric. Meteorol.*, *54*, 225–231.
- Habets, F., A. Boone, and J. Noilhan (2003), Simulation of a Scandinavian basin using the diffusion transfer version of ISBA, *Global Planet. Change*, *38*(1–2), 137–149.
- Heitman, J. L., X. Xiao, R. Horton, and T. J. Sauer (2008a), Sensible heat measurements indicating depth and magnitude of subsurface soil water evaporation, *Water Resour. Res.*, *44*, W00D05, doi:10.1029/2008WR006961.
- Heitman, J. L., R. Horton, T. J. Sauer, and T. M. Desutter (2008b), Sensible heat observations reveal soil-water evaporation dynamics, *J. Hydrometeorol.*, *9*(1), 165–171.
- Heitman, J. L., R. Horton, T. J. Sauer, T. S. Ren, and X. Xiao (2010), Latent heat in soil heat flux measurements, *Agric. For. Meteorol.*, *150*, 1147–1153.
- Heusinkveld, B., A. Jacobs, A. A. M. Holtslag, and S. Berkowicz (2004), Surface energy balance closure in an arid region: Role of soil heat flux, *Agric. For. Meteorol.*, *122*(1–2), 21–37.
- Holmes, T. R. H., M. Owe, R. A. M. de Jeu, and H. Kooi (2008), Estimating the soil temperature profile from a single depth observation: A simple empirical heatflow solution, *Water Resour. Res.*, *44*, W02412, doi:10.1029/2007WR005994.
- Horton, R., and P. Wierenga (1983a), Estimating the soil heat-flux from observations of soil-temperature near the surface, *Soil Sci. Soc. Am. J.*, *47*(1), 14–20.
- Horton, R., and P. Wierenga (1983b), Determination of the mean soil-temperature for evaluation of heat-flux in soil, *Agric. Meteorol.*, *28*(4), 309–319.
- Horton, R., P. Wierenga, and D. Nielsen (1983), Evaluation of methods for determining the apparent thermal-diffusivity of soil near the surface, *Soil Sci. Soc. Am. J.*, *47*(1), 25–32.
- Ibrom, A., E. Dellwik, H. Flyvbjerg, N. O. Jensen, and K. Pilegaard (2007), Strong low-pass filtering effects on water vapour flux measurements with closed-path eddy correlation systems, *Agric. For. Meteorol.*, *147*, 140–156.
- Idso, J., K. Aase, and R. D. Jackson (1975), Net radiation–soil heat flux relations as influenced by soil water content variations, *Boundary Layer Meteorol.*, *9*, 113–122.
- Jackson, R. D., P. Pinter, and R. Reginato (1985), Net-radiation calculated from remote multispectral and ground station meteorological data, *Agric. For. Meteorol.*, *35*, 153–164.
- Kun, Y., and J. Wang (2008), A temperature prediction-correction method for estimating surface soil heat flux from soil temperature and moisture data, *Sci. China, Ser. D*, *51*(5), 721–729.
- Massman, W. (1993), errors associated with the combination method for estimating soil heat-flux, *Soil Sci. Soc. Am. J.*, *57*(5), 1198–1202.
- Massman, W. (2000), A simple method for estimating frequency response corrections for eddy covariance systems, *Agric. For. Meteorol.*, *104*(3), 185–198.
- Massman, W., and X. Lee (2002), Eddy covariance flux corrections and uncertainties in long-term studies of carbon and energy exchanges, *Agric. For. Meteorol.*, *113*, 121–144.
- Mayocchi, C., and K. Bristow (1995), Soil surface heat-flux: Some general questions and comments on measurements, *Agric. For. Meteorol.*, *75*(1–3), 43–50.



- Meijninger, W., and H. De Bruin (2000), The sensible heat fluxes over irrigated areas in western Turkey determined with a large aperture scintillometer, *J. Hydrol.*, 229, 42–49.
- Meijninger, W., O. Hartogensis, W. Kohsiek, J. Hoedjes, R. Zuurbier, and H. De Bruin (2002), Determination of area-averaged sensible heat fluxes with a large aperture scintillometer over a heterogeneous surface: Flevo-land field experiment, *Boundary Layer Meteorol.*, 105(1), 37–62.
- Murray, T., and A. Verhoef (2007a), Moving towards a more mechanistic approach in the determination of soil heat flux from remote measurements: I. A universal approach to calculate thermal inertia, *Agric. For. Meteorol.*, 147, 80–87.
- Murray, T., and A. Verhoef (2007b), Moving towards a more mechanistic approach in the determination of soil heat flux from remote measurements: II. Diurnal shape of soil heat flux, *Agric. For. Meteorol.*, 147, 88–97.
- Ochsner, T. E., T. J. Sauer, and R. Horton (2006), Field tests of the soil heat flux plate method and some alternatives, *Agron. J.*, 98(4), 1005–1014.
- Ochsner, T. E., T. J. Sauer, and R. Horton (2007), Soil heat storage measurements in energy balance studies, *Agron. J.*, 99(1), 311–319.
- Paw, K., D. Baldocchi, T. Meyers, and K. Wilson (2000), Correction of eddy-covariance measurements incorporating both advective effects and density fluxes, *Boundary Layer Meteorol.*, 97(3), 487–511.
- Philip, J. (1961), Theory of heat flux meters, *J. Geophys. Res.*, 66(2), 571–579.
- Sakai, M., S. B. Jones, and M. Tuller (2011), Numerical evaluation of sub-surface soil water evaporation derived from sensible heat balance, *Water Resour. Res.*, 47, W02547, doi:10.1029/2010WR009866.
- Santanello, J., and M. Friedl (2003), Diurnal covariation in soil heat flux and net radiation, *J. Appl. Meteorol.*, 42(6), 851–862.
- Sauer, T. J., D. W. Meek, T. E. Ochsner, A. R. Harris, and R. Horton (2003), Errors in heat flux measurement by flux plates of contrasting design and thermal conductivity, *Vadose Zone J.*, 2(4), 580–588.
- Sauer, T. J., T. E. Ochsner, J. L. Heitman, R. Horton, B. D. Tanner, O. D. Akinoyemi, G. Hernandez-Ramirez, and T. B. Moorman (2008), Careful measurements and energy balance closure—The case of soil heat flux, paper presented at AMS Meeting, 28th Conference on Agricultural and Forest Meteorology, American Meteorological Society, Orlando, FL.
- Sayde, C., C. Gregory, M. Gil-Rodriguez, N. Tuffillaro, S. Tyler, N. van de Giesen, M. English, R. Cuenca, and J. S. Selker (2010), Feasibility of soil moisture monitoring with heated fiber optics, *Water Resour. Res.*, 46, W06201, doi:10.1029/2009WR007846.
- Spittelhouse, D., and T. Black (1981), Measuring and modeling forest evapo-transpiration, *Can. J. Chem. Eng.*, 59(2), 173–180.
- Stewart, J., and A. Thom (1973), Energy budgets in pine forest, *Q. J. R. Meteorol. Soc.*, 99(419), 154–170.
- Twine, T., W. Kustas, J. Norman, D. Cook, P. Houser, T. Meyers, J. Prueger, P. Starks, and M. Wesely (2000), Correcting eddy-covariance flux underestimates over a grassland, *Agric. For. Meteorol.*, 103(3), 279–300.
- Wang, J., and R. L. Bras (1999), Ground heat flux estimated from surface soil temperature, *J. Hydrol.*, 216(3–4), 214–226.
- Wang, L., Z. Gao, and R. Horton (2010), Comparison of six algorithms to determine the soil apparent thermal diffusivity at a site in the loess plateau of China, *Soil Sci.*, 175(2), 51–60.
- Wang, Z.-H., and E. Bou-Zeid (2011), Comment on “Impact of wave phase difference between soil surface heat flux and soil surface temperature on soil surface energy balance closure” by Z. Gao, R. Horton, and H. P. Liu, *J. Geophys. Res.*, 116, D08110, doi:10.1029/2010JD015117.
- Wang, Z.-H., and E. Bou-Zeid (2012), A novel approach for the estimation of soil ground heat flux, *Agric. For. Meteorol.*, 154–155, 214–221.
- Webb, E., G. Pearman, and R. Leuning (1980), Correction of flux measurements for density effects due to heat and water-vapor transfer, *Q. J. R. Meteorol. Soc.*, 106(447), 85–100.
- Wilson, K., et al. (2002), Energy balance closure at FLUXNET sites, *Agric. For. Meteorol.*, 113(1–4), 223–243, doi:10.1016/S0168-1923(02)00109-0.